Night-Time Light Imagery Reveals China's City Activity During the COVID-19 Pandemic Period in Early 2020

Ranyu Yin, Guojin He, Wei Jiang, Yan Peng, Zhaoming Zhang, Moxuan Li, and Chengjuan Gong

***Abstract*—The COVID-19 global pandemic has posed a serious impact on human life and health. Facing this unknown, unexpected, and devastating disease, China launched a resolute battle to prevent and control its spread. This study focused on assessing the recovery of city activity of 17 administrative regions in China around the COVID-19 pandemic period in early 2020. The night-time light (NTL) satellite remote sensing data, NPP-VIIRS dataset, was applied to evaluate the NTL changes during the coronavirus epidemic to understand the impact of the epidemic on city activity and the economy of China. A series of median composites was first constructed to analyze short-term NTL changes. Based on these median composites, the ratio map, difference map, wave index, and recovery ratio (RR) were defined to indicate the NTL recovery pattern and its spatial distribution characteristics. The results are as follows: first, the adopted median composites are able to describe the NTL changes in the short term; second, the recovery of city activity could not be exactly described by RR of a single year but could be evaluated by the comparison of RR between two adjacent years; third, a partial and spatially heterogeneous recovery of city activity is observed after the 2020 holiday compared to 2019, fourth, a better degree of recovery is observed after China announced its fully work resumption.**

Manuscript received March 5, 2021; revised April 14, 2021; accepted May 5, 2021. Date of publication May 7, 2021; date of current version May 27, 2021. This work was supported in part by the Strategic Priority Research Program of Chinese Academy of Sciences under Grant XDA19090300, and in part by the National Natural Science Foundation of China under Grant 61731022, Grant 61860206004, Grant 61701495, and Grant 41701468. *(Guojin He and Wei Jiang contributed equally to this work.) (Corresponding author: Guojin He.)*

Ranyu Yin and Chengjuan Gong are with the Aerospace Information Research Institute, Chinese Academy of Sciences, Beijing 100094, China, and also with University of Chinese Academy of Sciences, Beijing 100049, China (e-mail: yinry@aircas.ac.cn; gongcj@aircas.ac.cn).

Guojin He and Yan Peng are with the Aerospace Information Research Institute, Chinese Academy of Sciences, Beijing 100094, China, with the University of Chinese Academy of Sciences, Beijing 100049, China, with the Key Laboratory of Earth Observation Hainan Province, Sanya 572029, China, and also with the Sanya Institute of Aerospace Information Research Institute, Chinese Academy of Sciences, Sanya 572029, China (e-mail: hegj@aircas.ac.cn; pengyan@radi.ac.cn).

Wei Jiang is with the State Key Laboratory of Simulation and Regulation of Water Cycle in River Basin, China Institute of Water Resources and Hydropower Research, Beijing 100038, China, and also with the Remote Sensing Technology Application Center, Research Center of Flood and Drought Disaster Reduction of the Ministry of Water Resources, Beijing 100038, China (e-mail: jiangwei@iwhr.com).

Zhaoming Zhang is with the Aerospace Information Research Institute, Chinese Academy of Sciences, Beijing 100094, China, with the Key Laboratory of Earth Observation Hainan Province, Sanya 572029, China, and also with the Sanya Institute of Aerospace Information Research Institute, Chinese Academy of Sciences, Sanya 572029, China (e-mail: zhangzm@radi.ac.cn).

Moxuan Li is with the GEAR Lab, Texas A&M University, College Station, TX 77843 USA (e-mail: moxuan648709@tamu.edu).

Digital Object Identifier 10.1109/JSTARS.2021.3078237

***Index Terms*—COVID-19 pandemic, city activity, night-time imagery, satellite remote sensing, socioeconomic status, work resumption.**

I. Introduction

THE COVID-19 pandemic is a major public health emergency. As soon as cases of pneumonia of unknown cause were identified in Wuhan City, Hubei Province, China, acted immediately to conduct etiological and epidemiological investigations and to stop the spread of the disease, and promptly reported the situation. Through painstaking efforts and tremendous sacrifice, and having paid a heavy price, China, has succeeded in turning the situation around [1]. After February 11, 2020, with the exception of Hubei Province, the epidemic situation in numerous provinces was effectively controlled, as reported by the media. People gradually returned to work after the spring festival, a series of major national infrastructure projects resumed, and a gradual recovery in the Chinese economy was also underway. Understanding the scale and timing of the resumption of city activity and industrial production following the COVID-19 outbreak is critical to assess the economic losses and economic recovery related to the epidemic.

The time when COVID-19 spread in China coincided with the beginning of the Chinese New Year holiday, also called the spring festival holiday. Thus, the description of after "COVID-19" is equal to that after "the 2020 spring festival holiday." For consistency between 2019 and 2020, the description of "2020 spring festival holiday" is used in some parts of this article.

Remote sensing technology obtains information through noncontact methods to reflect the dynamic changes of surface elements, and has been proven to be large-scale, objective, and accurate [2], [3]. The night lighting of a city, resulting from the outdoor lighting of human activity at night [4], is a comprehensive indicator that can reflect the stage of economic development [5] and the degree of prosperity [6]. Two main kinds of long sequence night-time light satellite data exist, namely, Defense Meteorological Satellite Program Operational Linescan System (DMSP-OLS) and the Suomi National Polar-Orbiting Partnership Visible Infrared Imaging Radiometer Suite (NPP-VIIRS) [7]–[9]. Considering the ability of NTL data to allow the analysis of economic or social activity, and VIIRS can detect NTL at higher spatial and radiometric resolutions than DMSP-OLS and practically eliminates the problems of

TABLE I
PERIOD INFORMATION OF THE NTL DATA

Periods	Abbr.	Date Range	List of Year-DOY
Before 2019 Spring Festival holiday	B19	12/4/2018 – 12/17/2018	2018338, 2018340, 2018341, 2018345: 2018351
During 2019 Spring Festival holiday	D19	2/4/2019 – 2/10/2019	2019035: 2019039, 2019041
After 2019 Spring Festival holiday	A19	2/28/2019 – 4/5/2019	2019059, 2019060, 2019064: 2019067, 2019070: 2019073, 2019088, 2019089, 2019092: 2019095
Before 2020 Spring Festival	B20	12/24/2019 – 12/30/2019	2019358: 2019364
During 2020 Spring Festival holiday	D20	1/24/2020 – 1/30/2020	2020024: 2020030
After 2020 Spring Festival holiday	A20	2/16/2020 – 2/24/2020	2020047: 2020053
Post-COVID-19	P20	4/24/2020 - 4/30/2020	2020115, 2020118, 2020119, 2020121

saturation, blooming, and a lack of on-board calibration [10], the NPP-VIIRS data were adopted to trace the city activity changes during the COVID-19 epidemic.

The dimming of lights in China during the COVID-19 pandemic was assessed by Liu *et al.* and Elvidge *et al.* based on direct statistics or maps showing the monthly change in cloud-free VIIRS composites [11], [12], which indicated the feasibility of monitoring the decline and recovery in economic activity levels using NTL as a proxy [12]. However, the NTL recovery status was not able to be clearly quantified because the multitemporal change in radiance patterns could not be traced. For example, a decrease in NTL between period T1 and period T2 may represent an initial decrease followed by a partial recovery, which cannot be represented by the direct change maps. In addition, the changes of NTL in the short-term cannot be represented by monthly composites.

In this study, a series of short-term composite image are synthesized for analyzing short-term NTL changes, which could be flatten in monthly composites [13]. The median compositing method, which enables the efficient use of multitemporal data and cloud-gap filling, and has been widely used in land cover mapping [14]–[16], was adopted for generating short-term VIIRS composite images. Then, the wave index (WI) of VIIRS composites was defined to assess the NTL recovery status and the direct change analysis, i.e., ratio and difference, was also applied to examine the NTL change pattern. To examine the reliability of both the WI and the direct change analysis, the change patterns around the spring festivals of 2019 and 2020 were compared.

II. MATERIALS AND METHODS

A. Study Area and Data Source

The NTL changes of 17 administrative regions, see Section III-C2 for details, in the eastern and southern areas of China was assessed using VNP46A1 data products of NPP-VIIRS. The research area range is approximately from 20°N to 40°N, 110°E to 123°E, which is covered by four tiles of the Sinusoidal Tile Grid [17] of VNP46A1 data products.

The VNP46A1 product of NPP-VIIRS provides daily NTL data, collected by the day–night band (DNB) sensor, with a brightness intensity unit of $10^{-9}\,\mathrm{W}\cdot\mathrm{cm}^{-2}\cdot\mathrm{sr}^{-1}$ and a spatial resolution of approximately 500 m. The NTL data used in this article covering seven periods around the spring festival in 2019 and 2020 were collected to assess the city activity changes. The details of seven periods and the acquisition times of the NTL data are shown in Table I. For convenience, the short names in the column named "abbr." are used in the following text. The year and day-of-year (DOY) pairs of adopted data for every period are listed in the column "list of year-DOY" separated by commas, and the continuous DOYs are merged into the "Start: End" format.

The specific DOYs were manually derived based on visual examination to ensure a higher quantity of valid data in the composites (see Section II-B1). Data containing excessive extraneous features, such as moonlight and stray light (Elvidge *et al.*), were manually excluded by visual checking. The date range of the actual holiday may vary in different industries, but the holiday usually takes place for two weeks or less centered on the New Year date, that is, the first day of the lunar year. Typically, a national work stopping occurs before the holiday and the resumption after the holiday. Wuhan announced its reopening and China began to fully resume work on April 8, 2020; thus, the date range of post-COVID-19 period is selected after this.

Because the spring festival period for analyzing NTL data is a short period of seven days, other periods also adopted seven days of data for consistency. However, the date range of some periods was extended due to a lack of sufficient valid data using only seven days.

B. Methods

In this article, the median composites method is used to generate cloud-free NTL imagery for every period, the difference and ratio method is used to directly NTL change analyze, and the WI and the RR are defined to trace the process of NTL recovery. The overall workflow of this article is shown in Fig. 1. More details would be illustrated in the following sections.

1) NTL Data (VNP46A1) Preprocessing: Original DNB data may be subject to interference due to extraneous factors, such as clouds and moonlight, and thus, cannot be directly used to analyze a large area. To address this problem, this study generated synthesized images for multitemporal images in each of the periods listed in Table I. First, potential cloudy pixels were masked based on the corresponding cloud indexing band in each image, and then the median composite was constructed for each period.

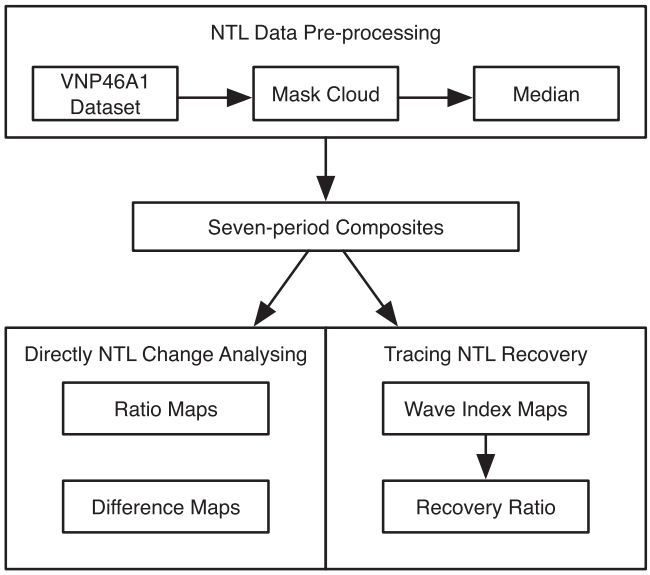

Fig. 1. Overall workflow chart.

In the cloud indexing band, the "cloud detection results and confidence indicator" (CRCI) are classed into the following four levels: confident clear, probably clear, probably cloudy, and confident cloudy, and the "cloud mask quality" (CQ) is ranked in the following four levels: high, medium, low, and poor [18].

Theoretically, using the strictest criterion to remove potential cloudy pixels could maximizes the reliability of the analysis of night light changes but limit the number of valid pixels. Thus, we employed a tradeoff in the synthesis of images, and retained the pixels for which the "CQ-CRCI" pairs were labeled "high-confident clear," "high-probably clear," and "medium-confident clear," to avoid cloud blocking while maximizing the coverage of valid data.

The median composite, which was also recently used to analyzing daily NTL data [19], was computed pixel-wise, such that each pixel in the output was composed of the median value of all of the valid images in the period at that location. The median composites of cloud-masked images can merge the valid pixels in all images of a period and lessen the impacts of thin cloud and other remaining extraneous features, before which most cloud pixels and images with significant extraneous features were already excluded. Thus, the composites could improve the reliability of NTL change analysis.

2) Directly Change Analyzing: The NTL changes between two periods could be described by the ratio or the difference of the NTL images of two periods. The ratio results of "during holiday/before holiday" (D/B) and "after holiday/before holiday" (A/B) of both 2019 and 2020 were calculated and referenced as "D/B 2019," "A/B 2019," "D/B 2020," and "A/B 2020," respectively. In addition, the ratio of "post-COVID-19/before holiday" of 2020 is also calculated and referenced as "P/B 2020" in the following. Similarly, the difference results of all these period pairs are also computed and referenced as "D-B 2019," "A-B 2019," "D-B 2020," "A-B 2020," and "P-B 2020" in the following text.

With reference to this work of Liu *et al.* [11], pixels with DNB radiance lower than $5 \cdot 10^{-9}\mathrm{W} \cdot \mathrm{cm}^{-2}\mathrm{sr}^{-1}$, which is the spectral range for vegetation, water, snow, and rural areas [20], were excluded from the computations. This policy was also adopted when calculating WI maps.

3) WI Calculation: As mentioned above, the change in NTL, from a decrease to an increase, may indicate a recovery of economic activity. To capture this change, we defined the NTL WI based on three-period observations, as shown in (1), which is computed pixel-wise during the three periods

$$\mathrm{WI} = (V_{\mathrm{after}} - V_{\mathrm{mid}})/(V_{\mathrm{before}} - V_{\mathrm{mid}}). \tag{1}$$

In (1), V_{before}, V_{mid}, and V_{after} represent the brightness values of before, mid, and after, respectively, in a three-period composite group. Theoretically, when the light recovers after the decrease, $\mathrm{WI} > 0$; the closer the recovery of the light to the previous light, the closer the WI value is to 1. For pixels with $V_{\mathrm{after}} < V_{\mathrm{mid}}$, WI was set to 0. Because the ratio index is particularly sensitive to noise when the denominator is small, it is necessary to avoid relatively small values of $V_{\mathrm{before}} - V_{\mathrm{mid}}$. Thus, we only calculated the WI values for pixels with $V_{\mathrm{before}} - V_{\mathrm{mid}} >= 2$. This threshold value was selected according to experience after data exploration and is illustrated in Section III-B. The threshold value ignores some pixels with low brightness or small changes in fluctuation, but it ensures the reliability of index results for relative analysis. In particular, when calculating the WI maps, only those pixels with DNB radiance greater than $5 \cdot 10^{-9}\mathrm{W} \cdot \mathrm{cm}^{-2}\mathrm{sr}^{-1}$ were adopted, as described in Section II-B1.

Specifically, in this article, the WIs of 2019 and 2020 were based on a three-period interval of before, during, and after the holiday, as listed in Table I, and the WI of post-COVID-19 was based on a three-period interval of B20, D20, and P20, as listed in Table I.

4) Regional Analyzing: To exploring the regional differences of NTL change pattern, two ratios are defined based on the results of directly NTL changes and WI.

The stable pixel ratio (SPR) is designed to evaluating the regional difference of directly NTL change, see the following:

$$\mathrm{SPR} = N_{\mathrm{stable}}/(N_{\mathrm{stable}} + N_{\mathrm{decrease}}). \tag{2}$$

N_{stable} and N_{decrease} indicate the number of pixels in areas with stable NTL and decreased NTL, respectively. The definitions of stable and decrease of NTL are illustrated in Section III-D. The sum of N_{stable} and N_{decrease} represent the total number of valid pixels. To avoid the problem of missing data, cities with $N_{\mathrm{stable}} + N_{\mathrm{decrease}} < 1000$ were excluded. A higher SPR indicates a smaller effect on city activity of COVID-19, and a more valid pixels indicate a bigger scale city.

The resume ratio (RR) is designed to evaluating the regional differences of the recovery of city activity, see the following:

$$\mathrm{RR} = N_{\mathrm{relight}}/(N_{\mathrm{relight}} + N_{\mathrm{off}}). \tag{3}$$

The N_{relight} indicates the total number of pixels in the area with $\mathrm{WI} >= 0.5$, assuming that these pixels may recover after the new year holiday; N_{off} indicates the total number of pixels in the area with $\mathrm{WI} < 0.5$, assuming that these pixels may not recover after the holiday.

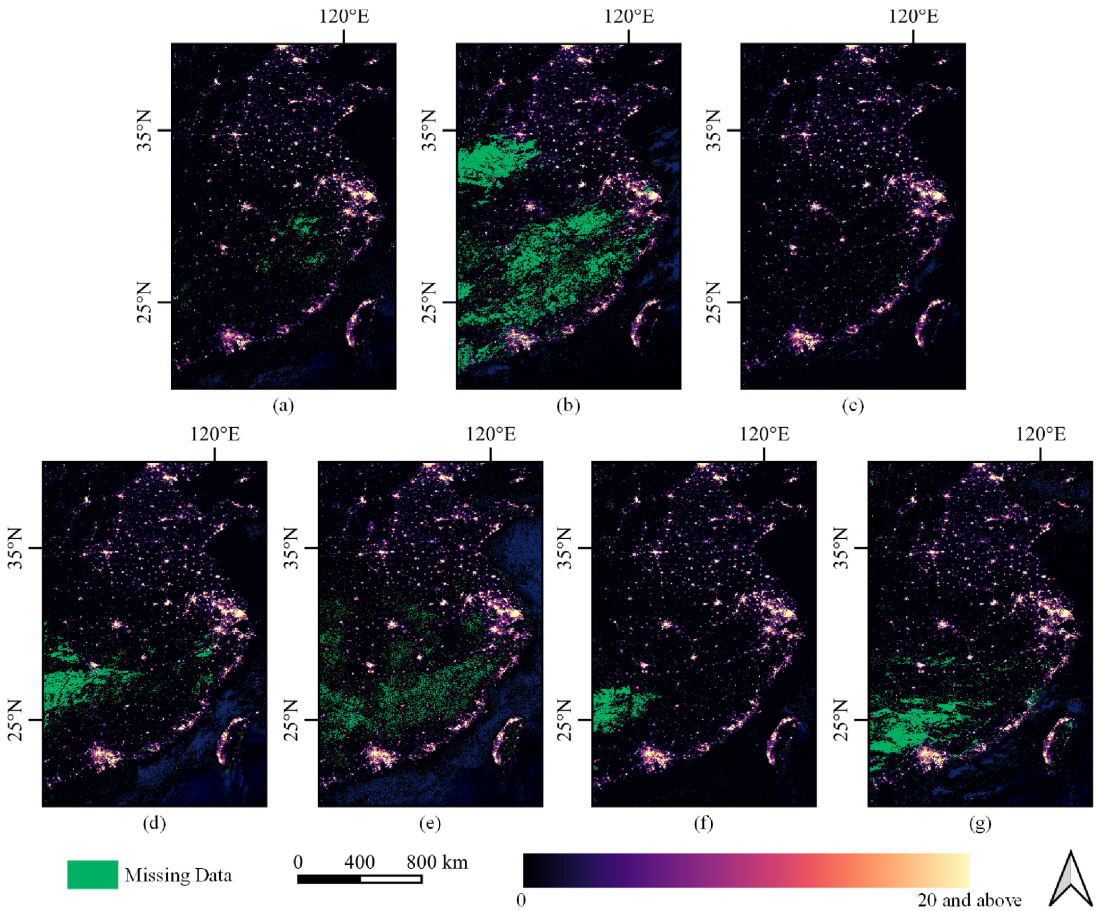

Fig. 2. DNB radiance of synthesized NTL images for seven periods (unit: $10^{-9}\mathrm{W}\cdot\mathrm{cm}^{-2}\mathrm{sr}^{-1}$). (a): B19, (b): D19, (c): A19, (d): B20, (e): D20, (f): A20, (g): P20. The pixels with a value above 20 are truncated to 20 when drawing these maps.

III. Results

A. Median Composites

Based on the NTL data listed in Table I, the median composites of all of the seven periods were synthesized and shown in Fig. 2, in which the green indicates the absence of valid data in the composites. It should be mentioned that impacts of extraneous features remain in the synthesized image, and are referred to as noise in the following discussion.

B. NTL Change Pattern Around the Spring Festival

The ratio maps of D/B and A/B of both 2019 and 2020 around Shanghai are shown as a sample in Fig. 3. Compared to the "before holiday period," the pixels of "during holiday" or "after holiday" with NTL increased more are redder and decreased more are more green. And the stable pixels tend to yellow.

The year 2019 is a normal year without the COVID-19 epidemic. In Fig. 3, compared to the A/B 2019(b), more pixels are NTL increased, in particular, decreased in the D/B 2019(a). This indicates a greater NTL change during the holiday and then a recovery after the holiday. Simultaneously, this proves the NTL resumption can be described by a comparison of the short-term median composites adopted in this article.

In contrast, for 2020, during the COVID-19 epidemic, more pixels in the D/B 2020(c) tend to stable or increased compared to 2019(a), showing a lower NTL reduction from before to during the holiday in 2020 compared to 2019, which may be because a large number of people stayed in the city rather than returning to their hometown. It may also be a result of community epidemic prevention, and the production and transportation of epidemic prevention materials. The A/B 2020(d) also shows a relatively smaller DNB radiance recovery after the holiday, which may indicate a partial city activity recovery.

Furthermore, for the whole research area described in Section II-A, the histograms of each ratio result were calculated, and are shown in Fig. 4; the ratio values above 2 were truncated to 2 when drawing histogram.

Similarly, for the whole research area, Fig. 4 also shows that

1) there are more pixels with NTL increase and particularly decrease more during the holiday (in D/B) than after the holiday (in A/B) in 2019;
2) there are less pixels with NTL decrease more (ratios lower than 0.7 approximately) during holiday in 2020 (D/B 2020) than in 2019 (D/B 2019);
3) there are more pixels during holiday with NTL close to before holiday (ratio range from 0.7 to 1.2 approximately) in 2020 (D/B 2020) than in 2019 (D/B 2019);

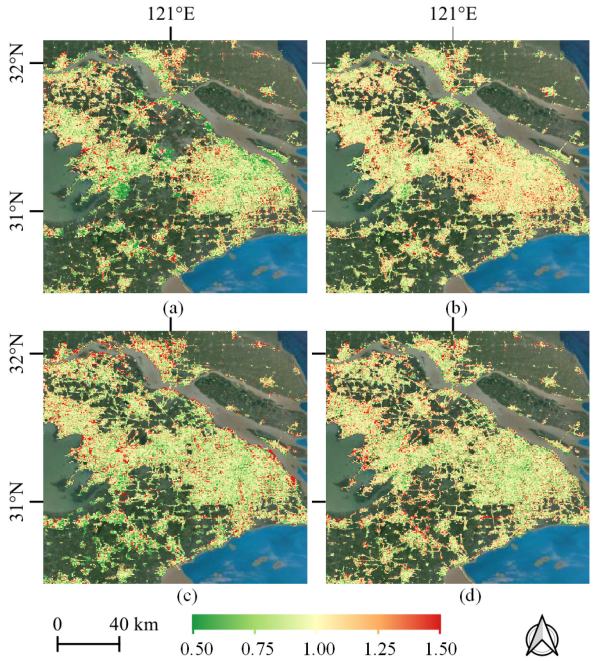

Fig. 3. Ratio maps of (a) D/B 2019, (b) A/B 2019, (c) D/B 2020, (d) A/B 2020. Base Map: Google Map. The ratio values below 0.5 and above 1.5 were truncated to 0.5 and 1.5, respectively, when drawing this map.

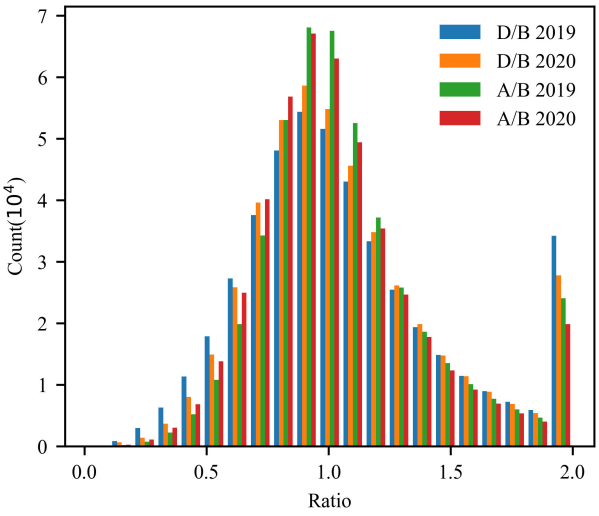

Fig. 4. Histograms of D/B and A/B results of 2019 and 2020; ratio values above 2 were truncated to 2 when drawing the histogram.

4) there are less pixels after holiday with NTL close to or greater than before holiday in 2020 (in A/B 2020) than 2019 (in A/B 2019).

These also indicate a lower level of NTL reduction during holiday and a partial NTL resumption after the holiday in 2020 for the overall research area like Fig. 3.

For the pixels in which the DNB radiance decreased from before to during the holiday, the histogram is shown in Fig. 5. Although the number of pixels with D/B ratios lower than 0.7 in 2019 is larger than that of 2020 in Fig. 4, the number of pixels with DNB radiance decreased by more than $2 \cdot 10^{-9}\mathrm{W} \cdot \mathrm{cm}^{-2}\mathrm{sr}^{-1}$ was smaller in 2019 than in 2020 in Fig. 5. This indicates that the DNB radiance of pixels with

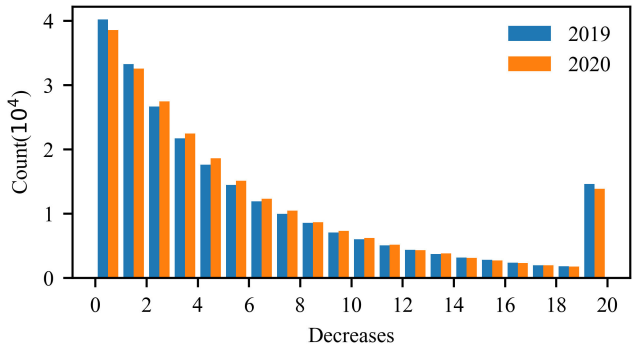

Fig. 5. Histograms of DNB radiance decreases from before the holiday (spring festival) to during the holiday in 2019 and 2020; values above 20 were truncated to 20 when drawing the histogram.

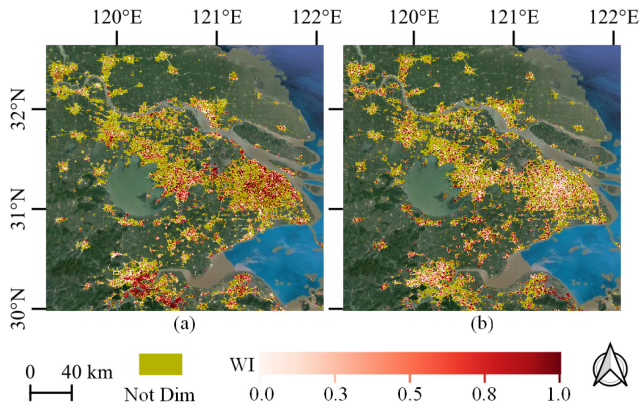

Fig. 6. Light WI map around Shanghai City. (a) 2019. (b) 2020.

relatively smaller values decreased more in 2019 than in 2020, and the pixels with closed commercial or industrial areas likely decreased by more than $2 \cdot 10^{-9}\mathrm{W} \cdot \mathrm{cm}^{-2}\mathrm{sr}^{-1}$. These pixels with relatively smaller values are likely to be residential areas [11], and this result could confirm that a large number of people stayed in the city, rather than returning to their hometown, and the impact of community epidemic prevention activity. As a result, those pixels with $V_{\mathrm{before}} - V_{\mathrm{mid}} < 2$ were excluded when deriving the WI.

C. *Tracing the NTL Recovery*

1) Results of WI: A WI value greater than 0 indicates that a change pattern in the NTL radiance from high (before the spring festival holiday) to low (during the spring festival holiday) to high (after the spring festival holiday) occurred. A smaller value means that there may be fluctuations caused by noise, or no significant recovery of city activity has occurred; higher WI values mean that there may be a recovery in city activity.

The WI maps were calculated for the whole research area and the results around Shanghai are shown in Fig. 6. The pixels with $V_{\mathrm{before}} - V_{\mathrm{mid}} < 2$ were excluded when counting, because they were regarded as not dim during the holiday, and are labeled in dark yellow. It is obvious that a larger number of pixels were red in 2019, Fig. 6(a), whereas more pixels tended to white in 2020, Fig. 6(b). For the whole research area, the histogram of WI is shown in Fig. 7, in which the number of pixels with a higher WI

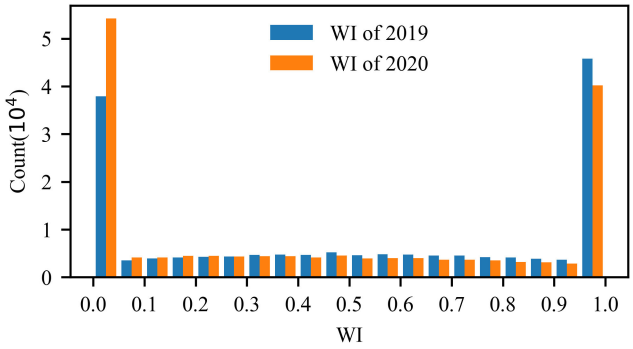

Fig. 7. Histogram of WI over whole research area in 2019 and 2020.

TABLE II
RR OF DIFFERENT REGIONS IN 2019 AND 2020

Region	RR 2019	RR 2020	Difference
Beijing City	68.8%	47.1%	-21.7%
Tianjin City	58.7%	45.3%	-13.4%
Hebei Province	54.4%	45.1%	-9.3%
Shanxi Province	46.8%	47.5%	0.7%
Shanghai City	73.0%	50.7%	-22.3%
Jiangsu Province	59.3%	57.0%	-2.3%
Zhejiang Province	63.3%	64.8%	1.4%
Anhui Province	65.7%	63.8%	-1.8%
Fujian Province	52.0%	42.5%	-9.5%
Jiangxi Province	88.2%	58.1%	-30.0%
Shandong Province	49.3%	53.1%	3.7%
Henan Province	67.5%	50.2%	-17.3%
Hubei Province	78.0%	42.7%	-35.3%
Hunan Province	70.6%	26.5%	-44.2%
Guangdong Province	62.8%	27.1%	-35.7%
Taiwan Province	40.9%	43.8%	2.9%
Hangkong District	53.6%	60.9%	7.3%

value in 2019 is obviously larger than that in 2020. Furthermore, there are a larger number of pixels with WI close to 0 in 2020.

In the WI maps, the trace of NTL recovery is visually emphasized. Specially, the work stopping and work resumption are two main events around holiday, and thus, the work resumption is strongly related to the trace of NTL recovery. The differences of WI between 2019 and 2020 indicate a partial work resumption after the spring festival holiday in 2020 compared to 2019.

2) Regional Difference of WI Results: To further quantify the recovery status in different regions, the RR of some regions of China based on WI 2019 and WI 2020 is calculated and listed in columns "RR 2019" and "RR 2020" of Table II. For convenience, the differences between "RR 2019" and "RR 2020" are also listed in the "difference" column of Table II.

Theoretically, if all of the NTL decreases are caused by the close of commercial and industrial place during holiday, and then recovered after the holiday ideally, the RR should be 100%. In fact, the NTL changes are not totally caused by the change of status of commercial and industrial operations, and there may be biases in the measured radiance. Thus, the absolute RR value is generally lower and somewhat insufficient to quantify the work resumption.

TABLE III
RECOVERY RATIO DIFFERENCES OF DIFFERENT REGIONS IN 2019 AND POST-COVID-19, 2020

Region	Difference-Holiday	Difference-POST
Beijing City	-21.7%	-37.3%
Tianjin City	-13.4%	-16.3%
Hebei Province	-9.3%	-16.7%
Shanxi Province	0.7%	5.4%
Shanghai City	-22.3%	-16.2%
Jiangsu Province	-2.3%	-0.9%
Zhejiang Province	1.4%	4.1%
Anhui Province	-1.8%	0.7%
Fujian Province	-9.5%	1.8%
Jiangxi Province	-30.0%	-17.9%
Shandong Province	3.7%	4.8%
Henan Province	-17.3%	-9.7%
Hubei Province	-35.3%	-29.4%
Hunan Province	-44.2%	-13.0%
Guangdong Province	-35.7%	4.2%
Taiwan Province	2.9%	3.3%
Hangkong District	7.3%	6.3%

Considering the main notable difference of city activity between 2019 and 2020 around the spring festival in China is the work stopping caused by the epidemic of COVID-19, and there may not have been many changes in commercial and industry areas from 2019 to 2020, thus, the differences between RR 2019 and RR 2020 could indicate the difference in the work-resumption status between two years in different regions. A value closer to zero or positive indicates a similar or better work-resumption status in 2020 compared to that of 2019, and a large negative value indicates a worse work-resumption status.

Some of those regions in Table II show a relative higher negative RR difference, for example, Hubei Province, Hunan Province, Henan Province, Jiangxi Province, Guangdong Province, Shanghai city, and Beijing city, indicating the city activity of these regions has not recovered to the level of 2019 and could still be under relative strict control. However, the RR of some regions may be unreliable due to the insufficient data, which will be discussed in Section IV-B. Generally, this result reveals the spatial heterogeneity of city activity resumption among different regions after the spring festival in 2020 due to the COVID-19 epidemic.

3) Post-COVID-19 Period: Corresponding recovery ratio of different regions was also calculated, referred to as RR-POST in the following discussion. The differences between RR-POST and RR 2019 are listed in the "difference-POST" column of Table III, and the differences between RR 2019 and RR 2020 in Table II are listed in the "difference-holiday" column of Table III. Comparison between the values of two columns shows that most values increased. It can be concluded that a greater degree of work resumption occurred in most cities, which is consistent with the progress of fully resuming work. In particular, for Guangdong Province, which has the largest number of factories and the greatest GDP in China relative to other provinces, the difference changes to 4.2% from −35.7%. Some regions, such as Beijing City, still have big negative difference, which may be due to the strict epidemic prevention and control measures.

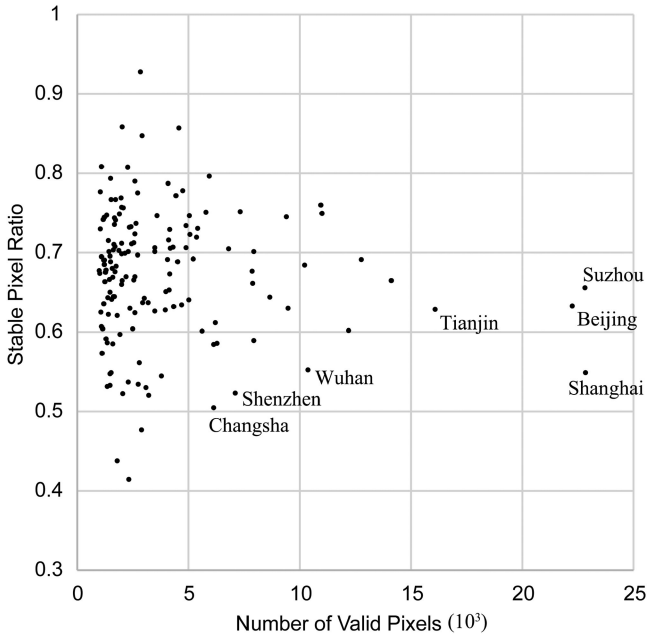

Fig. 8. Distribution of SPR.

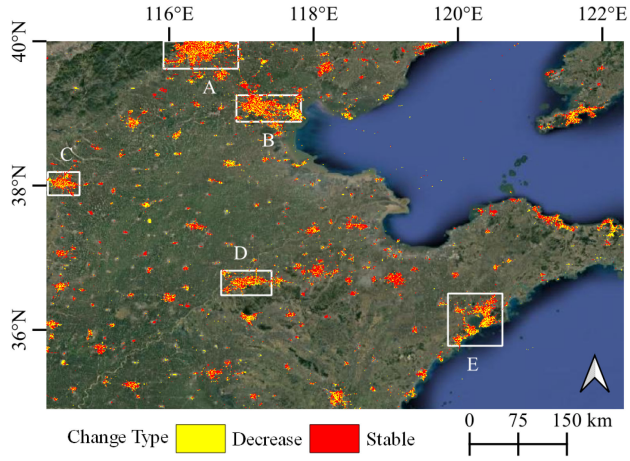

Fig. 9. Map of "A-B 2020" in the Bohai Economic Rim; (A: Beijing, B: Tianjin, C: Shijiazhuang, D: Jinan, E: Qingdao).

D. Spatial Heterogeneity of the Recovery of City Activity

This article concentrates on the recovery of city activity after the COVID-19 pandemic. The ratio results in Section III-B indicate that a partial recovery of city activity appears after the spring festival in 2020. And the results of RR in different regions reveal the spatial heterogeneity of the recovery of city activity. In this Section, more details of the city activity after the Spring Holiday in 2020 are discussed.

Considering the ratio map is not sensitive to the NTL changes of pixels with high DNB radiance and the WI map is not sensitive to those pixels not decreased during the holiday; the difference map, "A-B 2020," is used in this section. For visually convenience, the difference map is classified into two classes, "stable areas" with difference greater than or equal to $-2 \cdot 10^{-9}\mathrm{W} \cdot \mathrm{cm}^{-2}\mathrm{sr}^{-1}$ and "decrease areas" with difference lower than $-2 \cdot 10^{-9}\mathrm{W} \cdot \mathrm{cm}^{-2}\mathrm{sr}^{-1}$. This threshold value is based on the statistic in Section III-B.

The SPR in each city domain was counted to reveal the city-level NTL change difference. The distribution of SPR for 152 cities within the research area is shown in Fig. 8, in which the x-axis indicates the number of valid pixels and the y-axis indicates the SPR. City outliers are labeled with their name. Among the 152 cities, the number of $\mathrm{SPR} > 0.7$ is 61, accounting for 40.1%, and the number of $\mathrm{SPR} > 0.6$ is 126, accounting for 82.9%. In Fig. 8, cities with a higher SPR tend to be a smaller and the SPRs of large cities tend toward 0.6 approximately, which may indicate that many small cities were affected less by the COVID-19 epidemic and the large cities experienced COVID-19 impacts of similar magnitudes. This may be due to the fact that many people who return to their hometown for Chinese New Year during the holiday could not return in time due to the impact of the epidemic. However, it also shows that the distribution range of SPRs of smaller cities is bigger and that a lower SPR occurred in some smaller cities, indicating that a smaller city can be affected more and the situation of smaller cities under conditions of the COVID-19 epidemic varies.

1) NTL Changes of Urban Agglomerations: The Bohai Economic Rim refers to the coastal economic zone comprised largely of Liaodong Peninsula, Shandong Peninsula, and the Beijing–Tianjin–Hebei region. According to media reports on February 26, 2020, the resumption of work and production was progressing at that time throughout this region. Both epidemic prevention and resumption were appropriately processed. Most companies in commercial areas adopted flexible and online collaborative working models. Thus, the number of returning workers was limited and industrial production gradually resumed.

The results of the local NTL difference in the Bohai Economic Rim are shown in Fig. 9. The white boxes A, B, C, D, and E in the figure mark some of the major large cities in this region: Beijing, Tianjin, Shijiazhuang, Jinan, and Qingdao, respectively. In general, there are regional differences in the changes in the NTL of small and medium-sized towns. Most of the small and medium-sized towns appear as red "stable areas," which matches the conclusion of SPR analysis before.

For large cities, there are significant differences in the characteristics of NTL changes in different functional subregions within the city. Fig. 10 shows the changes of night lighting in various districts in large cities, and the industrial areas, residential areas, commercial office areas, and construction sites of Beijing, Tianjin, and Shandong were selected for comparison and analysis. The type of subregion in this study was determined by the main type of point of interest, which was manually checked using an online map service provided by AutoNavi Software Company Ltd., (Amap.com).

In Fig. 10, it was found that the areas experiencing a decrease in light are predominantly distributed in urban low-density residential areas, commercial and office areas, construction sites, etc. (see residential B and C, office/commercial, and construction). Stable areas are mostly distributed in industrial areas (see industry). This result indicates that the epidemic situation had a greater impact on the return of personnel in large cities, and that the resumption of production and business in commercial

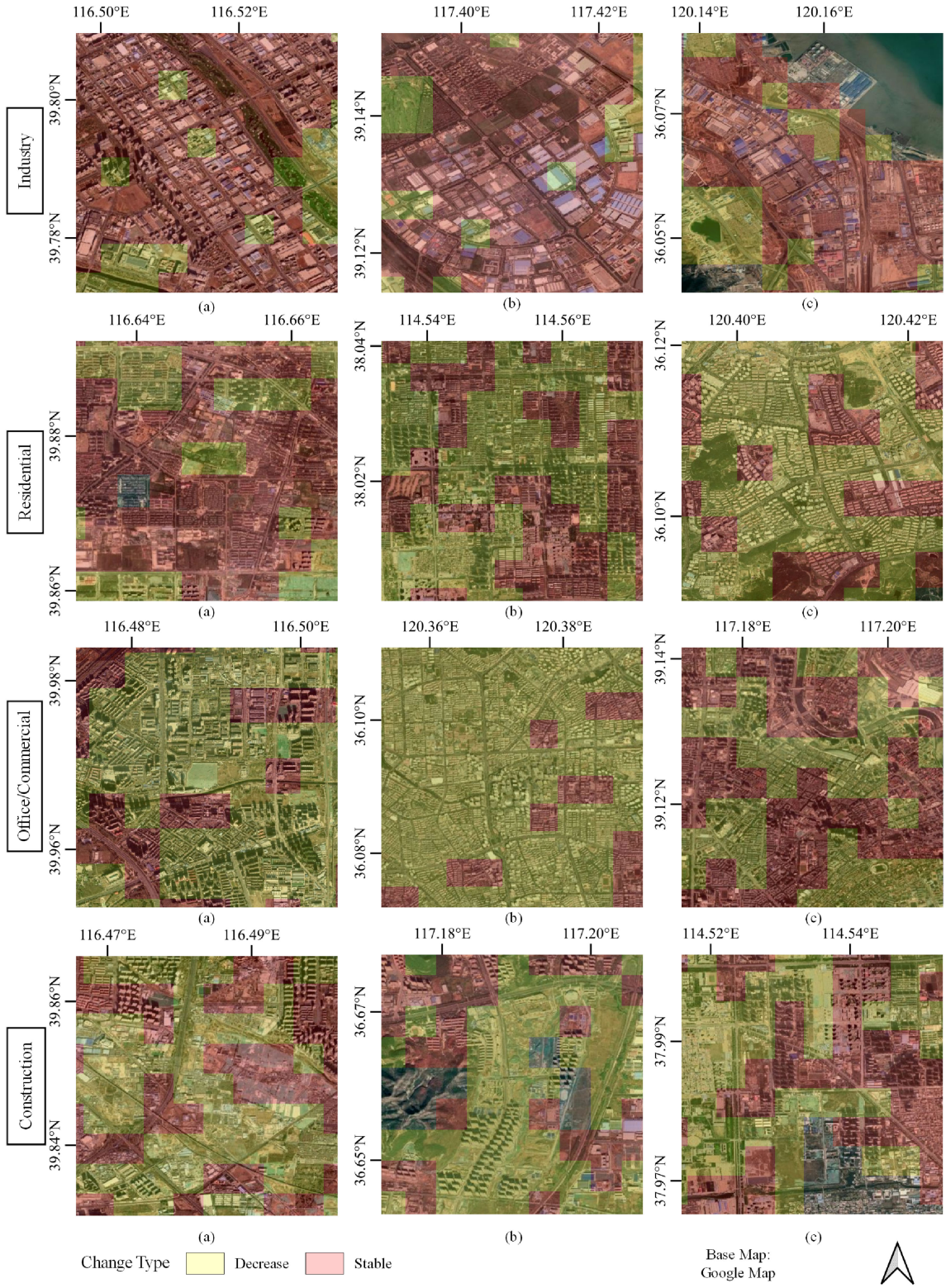

Fig. 10. Subregional changes of night lighting in cities.

and construction industries was somewhat delayed, but large industrial enterprises resumed production after the holidays.

The Yangtze River Delta Economic Belt is centered on Shanghai City, and comprises the cities of Anhui, Jiangsu, Zhejiang, and Shanghai. The result of the difference is shown in Fig. 11; similar to the case of the Bohai Economic Rim, the core areas in Shanghai, Hangzhou, Ningbo, and other cities have not yet fully recovered, which may be related to the fact that people who left during the spring festival have not returned, and large-scale enterprises have not resumed work.

The NTL recovery of the Pearl River Delta region shows a large difference among subregions and, overall, it also conforms

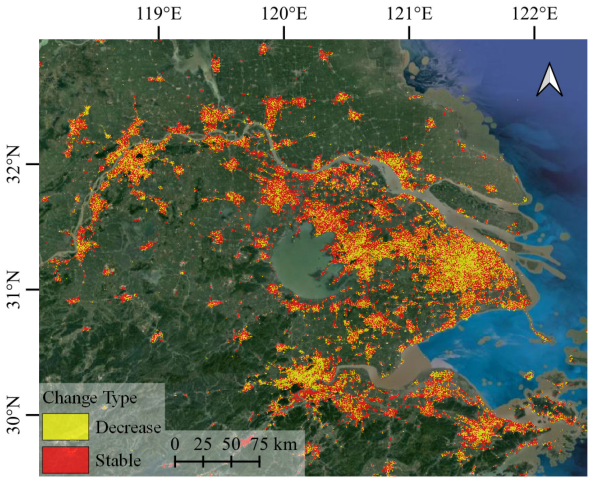

Fig. 11. Map of "A-B 2020" in the Yangtze River Delta Economic Belt.

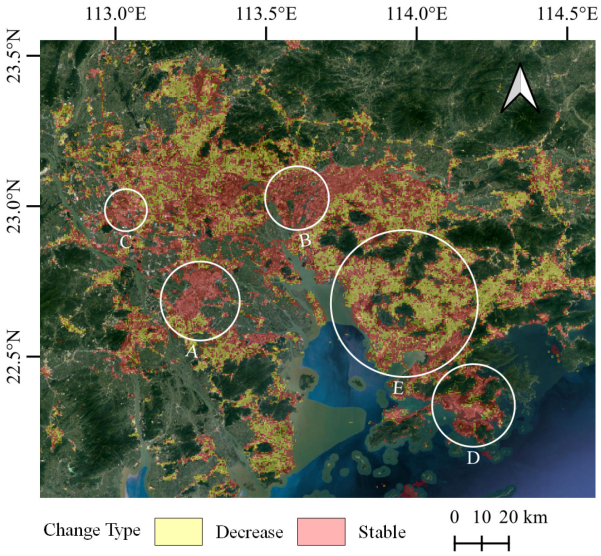

Fig. 12. Map of "A-B 2020" in the Pearl River Delta Economic Belt.

to the pattern that the NTL attenuated in the central area of the city and was stable in the industrial area. The difference image of NTL changes in this area is shown in Fig. 12, in which the white circle A marks the industrial clusters in Zhongshan and Foshan, B is the industrial cluster in Dongguan, and C is the industrial cluster in Foshan. These larger industrial agglomerations all show obvious "stable area" agglomerations, indicating that work has been resumed or not closed during holiday. In Shenzhen [see Fig. 12(E)], the NTL has decreased in most areas, mainly due to the nonreturn of the population in the area. The NTL in Hong Kong [see Fig. 12(D)] and Macau is stable, indicating that the Special Administrative Region cities have not been significantly affected by this epidemic.

2) Wuhan City: Wuhan City, Hubei Province, was the area that was most significantly affected by the coronavirus epidemic. However, from the image (see Fig. 13), the night lighting of Wuhan remained stable around the spring festival holiday of 2020 in some areas. This is because, from 10:00 on January 23, 2020, Wuhan's urban bus, subway, ferry, and long-distance

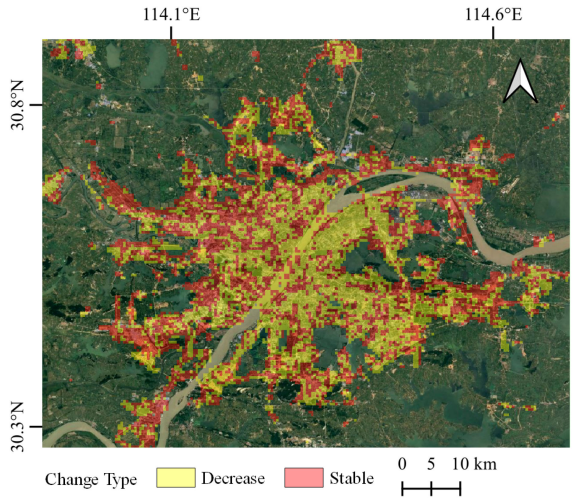

Fig. 13. Map of "A-B 2020" in Wuhan City, Hubei Province.

passenger transportation was suspended, citizens were not permitted to leave Wuhan, and the airport and railway station from the Han corridor were also temporarily closed. Therefore, after January 23, the net outflow population was relatively small. Conversely, the first medical team to assist Wuhan arrived in late January, and more than 10 000 doctors and nurses from across China travelled to Wuhan to provide assistance. In addition, the construction of Leishen Mountain Hospital and Huoshen Mountain Hospitals began in late January, and construction was carried out 24 hours per day. After February, a number of square cabin hospitals were opened and also operated 24 hours a day. These reasons could explain the stability and increase in the NTL in Wuhan around the spring festival holiday of 2020.

E. NTL Characters of Post-COVID-19 Period

The Pearl River Delta region is the main industry cluster of Guangdong Province, which shows a great RR difference changes in the Post-COVID-19 period. The comparisons of the ratio and difference change maps between after the 2020 spring festival holiday (A-B 2020 and A/B 2020) and post-COVID-19 (P-B 2020 and P/B 2020) in this region are shown in Fig. 14. It is clear that a large number of pixels marked as a decrease after the 2020 spring festival changed to stable in the difference results for post-COVID-19, and that the ratio result for most pixels is greater than 0.8, which indicates that the city activities have nearly fully recovered in this region.

IV. Discussion

A. Uncertainty Analyses

As mentioned above, the WI was computed only at the positions in which the images of all of the six periods have a valid pixel. Fewer valid pixels could increase the uncertainty when calculating the RR based on WI results. Except the lack of valid pixel, the low-quality valid pixels also bring uncertainty. The one key issue is that the potential cloudy pixels are not totally removed due to the tradeoff in Section II-B1 and the potential biases in CQ-CRCI, which could reduce the reliability of the

TABLE IV
DETAILS OF ROVP FOR DIFFERENT REGIONS (SEE ROVP-1 AND 2) AND AVERAGE NUMBER OF VALID OBSERVATIONS FOR DIFFERENT REGIONS IN SIX-PERIOD (SEE B19 TO A20)

Region	ROVP-1	ROVP-2	B19	M19	A19	B20	M20	A20
Beijing City	99.4%	56.7%	9.9	4.8	13.9	5.8	4.7	6.0
Tianjin City	98.2%	15.6%	8.3	4.8	13.6	5.4	4.1	5.7
Hebei Province	99.7%	50.8%	8.6	4.3	13.1	5.9	4.2	5.8
Shanxi Province	99.6%	39.4%	7.8	3.2	12.3	6.1	4.8	6.1
Shanghai City	95.3%	57.9%	3.9	2.2	6.9	3.0	2.6	6.8
Jiangsu Province	97.6%	68.2%	5.0	2.4	7.8	3.4	2.2	6.3
Zhejiang Province	77.7%	47.7%	2.7	1.9	5.6	2.2	2.2	5.1
Anhui Province	87.2%	59.7%	5.5	2.2	8.1	3.5	2.8	5.2
Fujian Province	65.7%	43.9%	4.2	2.6	4.2	3.2	3.5	5.5
Jiangxi Province	48.0%	18.0%	2.7	2.0	5.6	2.6	3.1	4.1
Shandong Province	99.1%	68.8%	8.0	3.6	12.4	3.7	2.8	5.5
Henan Province	69.8%	53.9%	7.1	2.3	10.1	4.6	4.1	5.1
Hubei Province	75.4%	48.0%	5.1	2.5	6.5	3.7	3.4	3.4
Hunan Province	48.7%	22.6%	2.7	1.8	5.3	1.7	3.7	3.0
Guangdong Province	75.3%	45.8%	3.9	2.6	5.3	4.4	3.1	6.0
Taiwan Province	84.7%	61.9%	4.4	3.9	4.5	2.8	2.6	4.9
Hangkong District	82.1%	19.7%	4.2	3.1	5.5	3.4	2.9	6.3

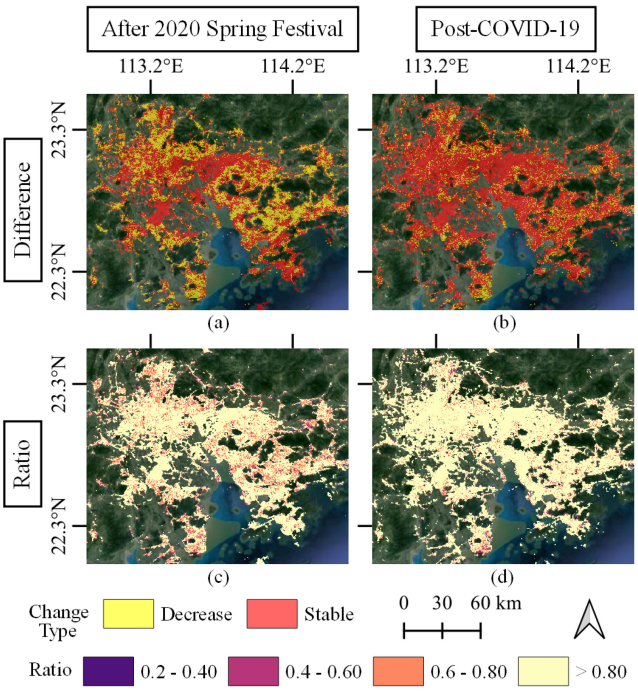

Fig. 14. Comparisons of difference and ratio between before the 2020 spring festival holiday and post-COVID-19.

composites and then the WI results. The other key issue is that there may be not sufficient observations in one period to lessen the impacts of extraneous features when generating composites.

To quantify the uncertainty, the ratio of the valid pixels (ROVP) participating in the calculation for each region and the average number of valid observations for different regions in six-period are calculated and shown in Table IV. The ROVP of the dataset adopting data in three CQ-CRCI levels as described in Section II-B1 is shown in column ROVP-1. And, specially, the ROVP of the dataset adopting only data with CQ-CRCI labeled "high-confident clear," which means the strictest policy, is shown in column ROVP-2.

In Table IV, some regions have a relatively higher ROVP-1 value but have an apparently lower ROVP-2 value, for example, Beijing, Tianjin, and Hebei, which indicates that there is a considerable part of these regions affected by potential cloudy pixels. In terms of the average number of valid observations, some regions at a certain period have a relatively lower value, even less than two, indicating that the corresponding composite in these regions could be affected by more extraneous features and then the WI results could be more biases.

B. *Performance of Short-Term Composites*

The monthly NTL composites have been used to exploring the NTL changes during the COVID-19 pandemic by much research. For example, Elvidge *et al.* found that the NTL decreased significantly from December 2019 to February 2020 based on the monthly composites [12]. However, February 2020 contains the spring festival holiday, and specially, the holiday was extended by the Chinese government to avoid the spread of COVID-19. In such a situation, the NTL in the composite of February 2020 is certain lower due to containing more holidays. In fact, the partial recovery of NTL is observed on the later February 2020 in this article. Although the short-term NTL composites could reveal the changing pattern closer to the real, the clouds and other extraneous features restrict its reliability, and it is still hard to precisely trace the short-term NTL changes, especially on a large scale.

C. *Wave Index*

Similarly, Lan *et al.* also analyze the city activities under the COVID-19 pandemic use the short-term NTL data and reveal a city activity partial recovery by directly comparing the NTL

between 2019 and 2020 of the same lunar date [21]. It is hard to compare the results in quantity with this article due to the method's different mechanisms. However, the NTL changes pattern in the real world could be complex, and both decreases and increases could happen around the spring festival. Thus, the total radiance of a region could omit some decreases due to others' increases in the same region. Furthermore, it could not distinguish between the simple decrease and the partial recovery following a decrease. Although the WI could quantify the change trace, the poor data availability and the accumulated error from multiperiod restrict its practicability and reliability. And the absolute values of RR also show impractical in this article. The performance of WI could be further evaluated by a long time series analyze.

V. Conclusion

This study focused on assessing the resumption of city activity in China's eastern and southern areas around the COVID-19 pandemic period in early 2020 using NTL remote sensing data.

The change in industries' operating status may cause a change in NTL radiance, and many researchers have demonstrated the relationship between NTL and human or economic activity. The DNB data of the VNP46A1 product were used to analyze NTL, and median composite images were synthesized for each period to avoid the impacts of clouds and extraneous features. Both the change trace and the direct change status during the COVID-19 outbreak were analyzed to assess city activity changes using NTL remote sensing data.

By comparing the DNB data directly around the spring festival holiday, it shows that

1) the NTL for most of China did not decrease significantly after the holiday, indicating that city activity was not seriously affected by the COVID-19 epidemic,
2) a series of short-term median composites can describe the NTL resumption;
3) a partial NTL resumption was observed after the spring festival in 2020, which was related to the resumption of work.

The change trace at a location (a pixel) was quantified by the proposed WI, calculated from three-period median DNB composites. Furthermore, the change trace of a region was quantified by the RR. Although the absolute value of RR in quantifying the resumption of city activity was not good, the difference compared to the adjacent year was found to indicate the recovery status.

The results of WI and RR show an apparent difference in the light recovery status between the spring festival holidays of 2019 and 2020, which indicates that the novel coronavirus epidemic had a more significant impact on China's economy. Also, it shows the spatial heterogeneity of the recovery of city activity in China; some provinces with lower disruption due to COVID-19 have lower RR differences, indicating a better recovery.

The results of the difference and SPR reveal that 1) some areas had yet to recover fully, including new City Development Areas, major infrastructure construction areas, and the cores of large cities; and 2) there were significant differences in the change of night lighting between large cities and small or medium cities. In contrast, the NTL of industrial manufacturing cluster areas of most cities remained stable or had recovered. The Yangtze River Delta urban agglomeration showed a better NTL recovery by February 24, followed by the Beijing–Tianjin–Hebei urban agglomeration. Most cities in the Pearl River Delta region also exhibited a good recovery, whereas Shenzhen had yet to recover. The NTL of the post-COVID-19 period may indicate a high degree of city activity or even work resumption in China.

The NTL data used in this article are subject to uncertainty due to the relatively low spatial resolution used to distinguish the precise location of light changes, the complex mechanism of light changing in reality, and particularly the data availability. The time when COVID-19 begin to spread in China coincided with the spring festival holiday, which allows the comparison with a regular national work stopping in this article. However, it also means that it could be more difficult if evaluating changes of city activity standalone. Data related to power consumption, offline payments, or public transit may allow direct assessment of the work-resumption status. However, these data are usually not freely or openly available, which limits such applications.

References

[1] The State Council Information Office of the People's Republic of China, "Fighting Covid-19 China in Action," Feb 2020. [Online]. Available: http://english.scio.gov.cn/whitepapers/2020-06/07/content_76135269_4.htm

[2] G. He *et al.*, "Processing of earth observation big data: Challenges and countermeasures," *Kexue Tongbao/Chinese Sci. Bull.*, vol. 60, no. 5/6, pp. 470–478, Feb. 2015.

[3] W. Jiang *et al.*, "Multilayer perceptron neural network for surface water extraction in Landsat 8 OLI satellite images," *Remote Sens.*, vol. 10, no. 5, 2018.

[4] W. Jiang *et al.*, "Potentiality of using Luojia 1-01 nighttime light imagery to investigate artificial light pollution," *Sensors*, vol. 18, no. 9, p. 2900, Sep. 2018. [Online]. Available: http://www.mdpi.com/1424-8220/18/9/2900

[5] S. Keola, M. Andersson, and O. Hall, "Monitoring economic development from space: Using nighttime light and land cover data to measure economic growth," *World Develop.*, vol. 66, pp. 322–334, Feb. 2015.

[6] Y. Zhou, T. Ma, C. Zhou, and T. Xu, "Nighttime light derived assessment of regional inequality of socioeconomic development in China," *Remote Sens.*, vol. 7, no. 2, pp. 1242–1262, Jan. 2015. [Online]. Available: http://www.mdpi.com/2072-4292/7/2/1242

[7] W. Jiang *et al.*, "Characterizing light pollution trends across protected areas in China using nighttime light remote sensing data," *ISPRS Int. J. Geo-Inf.*, vol. 7, no. 7, p. 243, Jun. 2018. [Online]. Available: http://www.mdpi.com/2220-9964/7/7/243

[8] W. Jiang, G. He, T. Long, C. Wang, Y. Ni, and R. Ma, "Assessing light pollution in China based on nighttime light imagery," *Remote Sens.*, vol. 9, no. 2, p. 135, Feb. 2017. [Online]. Available: http://www.mdpi.com/2072-4292/9/2/135

[9] W. Leng, G. He, and W. Jiang, "Investigating the spatiotemporal variability and driving factors of artificial lighting in the Beijing-Tianjin-Hebei region using remote sensing imagery and socioeconomic data," *Int. J. Environ. Res. Public Health*, vol. 16, no. 11, p. 1950, Jun. 2019. [Online]. Available: https://www.mdpi.com/1660-4601/16/11/1950

[10] M. M. Bennett and L. C. Smith, "Advances in using multitemporal night-time lights satellite imagery to detect, estimate, and monitor socioeconomic dynamics," *Remote Sens. Environ.*, vol. 192, pp. 176–197, Apr. 2017.

[11] Q. Liu *et al.*, "Spatiotemporal patterns of COVID-19 impact on human activities and environment in Mainland China using nighttime light and air quality data," *Remote Sens.*, vol. 12, no. 10, p. 1576, May 2020. [Online]. Available: https://www.mdpi.com/2072-4292/12/10/1576

[12] C. D. Elvidge, T. Ghosh, F.-C. Hsu, M. Zhizhin, and M. Bazilian, "The dimming of lights in china during the COVID-19 pandemic," *Remote Sens.*, vol. 12, no. 17, 2020. [Online]. Available: https://www.mdpi.com/2072-4292/12/17/2851

[13] C. D. Elvidge, K. Baugh, M. Zhizhin, F. C. Hsu, and T. Ghosh, "VIIRS night-time lights," *Int. J. Remote Sens.*, vol. 38, no. 21, pp. 5860–5879, Nov. 2017. [Online]. Available: https://www.tandfonline.com/doi/full/10.1080/01431161.2017.1342050
[14] P. Teluguntla *et al.*, "A 30-m landsat-derived cropland extent product of australia and china using random forest machine learning algorithm on Google earth engine cloud computing platform," *ISPRS J. Photogrammetry Remote Sens.*, vol. 144, pp. 325–340, Oct. 2018.
[15] X. Zhang *et al.*, "Rapid generation of global forest cover map using landsat based on the forest ecological zones," *J. Appl. Remote Sens.*, vol. 14, no. 2, 2020, Art. no. 022211.
[16] L. Carrasco, A. O'Neil, R. Morton, and C. Rowland, "Evaluating combinations of temporally aggregated Sentinel-1, Sentinel-2 and Landsat 8 for land cover mapping with Google Earth Engine," *Remote Sens.*, vol. 11, no. 3, p. 288, Feb. 2019. [Online]. Available: http://www.mdpi.com/2072-4292/11/3/288
[17] "LP DAAC - MODIS Overview." Accessed: May 20, 2021. [Online]. Available: https://lpdaac.usgs.gov/data/get-started-data/collection-overview/missions/modis-overview/#modis-tiling-systems
[18] M. O. Román *et al.*, "NASA's black marble nighttime lights product suite," *Remote Sens. Environ.*, vol. 210, pp. 113–143, Jun. 2018.
[19] Z. Zheng, Z. Wu, Y. Chen, G. Guo, Z. Yang, and F. Marinello, "A simple method for near-real-time monthly nighttime light image production," in *IEEE Geosci. Remote Sens. Lett.*, to be published. [Online]. Available: https://ieeexplore.ieee.org/document/9366332/
[20] T. Ma, "An estimate of the pixel-level connection between visible infrared imaging radiometer suite day/night band (VIIRS DNB) nighttime lights and land features across china," *Remote Sens.*, vol. 10, no. 5, p. 723, May 2018. [Online]. Available: http://www.mdpi.com/2072-4292/10/5/723
[21] T. Lan, G. Shao, L. Tang, Z. Xu, W. Zhu, and L. Liu, "Quantifying spatiotemporal changes in human activities induced by COVID-19 pandemic using daily nighttime light data," *IEEE J. Sel. Topics Appl. Earth Observ. Remote Sens.*, vol. 14, pp. 2740–2753, 2021.

Ranyu Yin was born in Shandong, China, in 1995. He received the B.E. degree in remote sensing from the China University of Geosciences, Wuhan, China, in 2016. He is currently working toward the Ph.D. degree in cartography and geographic information systems with the Aerospace Information Research Institute, Chinese Academy of Sciences (CAS), Beijing, China.

Guojin He was born in Fujian, China, in 1968. He received the B.Sc. degree in geology from Fuzhou University Fuzhou, China, in 1989, the M.Sc. degree in remote sensing of geology from the China University of Geosciences, Wuhan, China, in 1992, and the Ph.D. degree in geology from the Institute of Geology, Chinese Academy of Sciences (CAS), Beijing, China, in 1998.

From 1992 to 2007, he was with the Information Processing Department, China Remote Sensing Satellite Ground Station (RSGS), CAS, where he became the Deputy Director in 2001. From 2004 to 2008, he was a Professor and the Director of the Information Processing Department, RSGS. He was also the Head of the Research Group of Remote Sensing Information Mining and Intelligent Processing, Beijing, China. From 2008 to 2012, he was a Professor and the Director of the Value-added Product Department and the Deputy Director of the Spatial Data Center, Center for Earth Observation and Digital Earth, CAS. Since 2013, he has been a Professor and the Director of the Satellite Data Based Value-added Product Department and the Deputy Director of RSGS, Institute of Remote Sensing and Digital Earth (now is called Aerospace Information Research Institute), CAS. A large part of his earlier research dealt with information processing and applications of satellite remote sensing data. His research interests are focusing on big remote sensing data intelligence as well as using information retrieved from satellite remote sensing images, in combination with other sources of data to support better understanding of the earth.

Wei Jiang was born in Hubei, China, in 1991. He received the B.Sc. degree in remote sensing from Fujian Normal University, Fuzhou, China, in 2013 and the M.Sc. and Ph.D. degrees in cartography and geographic information systems from the Institute of Remote Sensing and Digital Earth, Chinese Academy of Sciences (CAS), Beijing, China, in 2016 and 2019, respectively.

In 2019, he joined the Research Center of Flood and Drought Disaster Reduction of the Ministry of Water Resources, China Institute of Water Resources and Hydropower Research, as an Engineer. His current research interests include hydrology remote sensing and nighttime light remote sensing.

Yan Peng was born in Hunan, China, in 1988. She received the B.S. degree in mineral resources engineering 2010 from the University of South China, Hengyang, Hunan, China and the M.S. degree in surveying and mapping engineering 2013 from Institute of Remote Sensing and Digital Earth, Chinese Academy of Science (CAS), Beijing, China, where she has been working toward the Ph.D. degree in cartography and geographic information systems with the Aerospace Information Research Institute since September 2019.

She joined the Institute of Remote Sensing and Digital Earth, CAS, as a Research Assistant in 2013. Her current research interests are atmospheric correction, mineral resources remote sensing, and target recognition.

Zhaoming Zhang received the B.Sc. degree in geographic information system from Henan University, Kaifeng, China, in 2003, the M.Sc. degree in satellite image processing from China Remote Sensing Satellite Ground Station, Chinese Academy of Sciences (CAS), Beijing, China, in 2006, and the Ph.D. degree in cartography and geographic information system from the Institute of Remote Sensing Applications, CAS, in 2009.

He has authored or coauthored more than 50 peer-reviewed articles and holds more than ten national invention patents. His research interests include information extraction from satellite image and remote sensing applications.

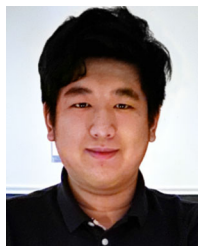

Moxuan Li was born in Hangzhou, China, in 1998. He received the B.S. degree in geographic information science from Ohio State University, Columbus, OH, USA, in 2020. He is currently working toward the M.S. degree in geography with the GEAR Lab, Texas A&M University, College Station, TX, USA.

Due to his study on GIS and his research related to forest fire during the internship, Moxuan's analysis interest is primarily on building tools for tracing and monitoring natural disasters and environmental changes. He aims to apply geostatistics and programming on social media data mining, and assess the disasters in certain areas, thus helping social managers develop disaster warning and response plans.

Chengjuan Gong was born in Hebei, China, in 1992. She received the B.E. degree in surveying and mapping engineering from the Xi'an University of Science and Technology, Xi'an, China, in 2016. She is currently working toward the Ph.D. degree in cartography and geographic information systems with the Aerospace Information Research Institute, Chinese Academy of Sciences (CAS), Beijing, China.